Thin Solid Films 693 (2020) 137702

Contents lists available at ScienceDirect

Thin Solid Films

journal homepage: www.elsevier.com/locate/tsf

A three-dimensional network of graphene/silicon/graphene sandwich sheets as anode for Li-ion battery

Zhijun Feng[a], Chenhui Huang[a], Ang Fu[a], Lun Chen[a], Fei Pei[a], Yanling He[b], Xiaoliang Fang[a], Baihua Qu[a], Xinyi Chen[a,*], Alan M.C. Ng[b,*], Jingqin Cui[a,*]

[a] Pen-Tung Sah Institute of Micro-Nano Science and Technology, Xiamen University, Xiamen 361005, China
[b] Department of Physics, South University of Science and Technology, Shenzhen 518055, China

ARTICLE INFO

Keywords:
3D Graphene
Pulverization
Silicon anode
Lithium-ion battery

ABSTRACT

A freestanding porous three-dimensional (3D) network composed of graphene/silicon/graphene sandwich sheets is proposed to prevent the expansion induced pulverization for Si-based anode in a lithium-ion battery. The architecture ensures the attachment of Si active material, improves the conductivity, and absorbs the Si volume expansions. The 3D Graphene and Si in this architecture work synergistically to contribute to the capacity, while the nanoscale of Si lowers the expansion during lithiation. And the 3D graphene with an interconnected skeleton, in addition to active material, also acts as the current collector as well as a stable support for Si.

1. Introduction

The increasing desires for ultrathin, flexible and portable electronic devices demand the improved energy density and long-term retention of lithium-ion batteries [1]. A promising anode material by forming Li alloys, silicon, however, faces enormous volume changes resulting in crumbling and cracking [2]. Hence, a stable and well performing Si-based electrode requires a low expansive presence of Si material, as well as stabilizing and buffering supports in configuration design to avoid expansion implicated pulverization [3–5]. With that in mind, several varieties of strategies have been developed for the protection of Si-based anodes. Firstly, nanosized hybrid materials such as Si/C were prepared to lower the volume variation and increase the whole electrochemical performance [5]. Secondly, conformal core-shell, hierarchical or sandwich structure was developed as a buffer to protect Si from pulverization and alleviate the volume variation [6–8]. In addition, elastic polymer binders had been employed to restrain the expansion and pulverization [9].

Following these principles, this work develops a Si/C hybrid network as the anode for lithium-ion batteries, combining sandwich configuration and three-dimensional graphene (3DGr) [8,10] The Si/C hybrid network, presenting as graphene/Si/graphene (3DGrSiGr) as Fig. 1 indicates, build up a microscale sandwich structure on the surface of 3DGr by embedding discontinuous Si nanoparticles on the surface of 3DGr and covering that with another graphene layers, The chemical vapor deposited (CVD) 3DGr forms an interconnected skeleton, acting as both an active material and a buffering support and current collector for Si [11,12], while Si nanoparticles further contribute to the electrochemical performance. Moreover, the 3DGr would contain more morphological defects such as wrinkles and cracks compared to flat graphene [13], which might provide additional sites to settle Si nanoparticles. In the proposed configuration, the small sizes of Si nanoparticles, the flexibility, porous 3D structure and morphological defects of 3DGr act synergistically to avoid pulverization for such a Si-based anode and thus facilitate the cycling stability.

2. Experimental

3DGr was fabricated following the Ni-sacrificing method via CVD [13]. A large sheet of Ni foam was loaded into the CVD tube and N_2, CH_4, H_2 were introduced at a flow ratio of 400:50:50 sccm. CH_4 decomposed at 1000 °C and few-layer graphene was obtained from the cooling process. Ni was then removed via soaking in 10% (w/v) nitric acid overnight followed by thorough washing with DI-water, leaving 3D graphene with a same skeleton. Silicon was deposited via magnetron sputtering and followed by another CVD process. Elemental, morphological and structural properties were characterized via scanning electron microscopy (SEM, Zeiss Supra 55, sampling at 10 kV) equipped with energy dispersive spectroscopy (EDS, Oxford, AZtec X-Max 80, sampling at 20 kV), high-resolution transmission electron microscopy (HRTEM, JEOL 2100F), X-ray diffraction (XRD, XRD-7000) and Raman spectroscopy (IDSpec ARCTIC, using 532 nm laser source). The electric

* Corresponding authors.
E-mail addresses: chenxinyi@xmu.edu.cn (X. Chen), ngamc@sustc.edu.cn (A.M.C. Ng), jqcui@xmu.edu.cn (J. Cui).

https://doi.org/10.1016/j.tsf.2019.137702
Received 19 March 2019; Received in revised form 6 October 2019; Accepted 15 November 2019
Available online 17 November 2019
0040-6090/ © 2019 Elsevier B.V. All rights reserved.

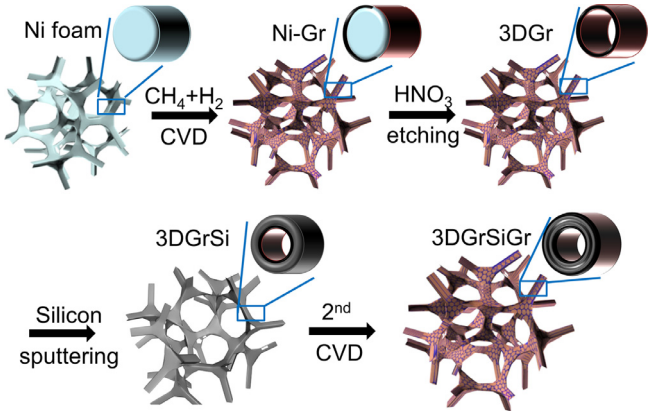

Fig. 1. Schematic 3DGrSiGr fabrication process.

structure was further studied via X-ray photoelectron spectra (XPS, ESCALAB 250xi) under an incident Al Kα radiation with the photon energy of 1486.6 eV over a circular area of diameter 500 μm. The spectra were processed with CasaXPS software (Casa Software Ltd.) employing a Shirley background correction. The peak deconvolution was performed using the CasaXPS software, fitting multiple Gaussian-Lorentzian components in the ratio of 85:15. The C1s binding energy of 284.8 eV was used as energy reference.

Weight difference of the sheet before and after sputtering was assumed as the Si mass loading. The prepared 3DGrSiGr (10–14 wt% of Si) was then cut into circular disks of diameter 1.10 cm and of an average weight 0.35 ± 0.03 mg. Higher areal density of silicon can be achieved by pressing several 3DGrSiGr together. The disks, several stacked together to remove the excessive voids, were assembled into CR2032 coin cells with lithium counter electrodes and Celgard 2400 separators. The electrolyte was 1 M $LiPF_6$ in ethylene carbonate/dimethyl carbonate (EC/DMC 1:1 in volume). The dis-/charging process was repeated at room temperature on a Neware BTS4000 battery testing system (Shenzhen, China) between 3.00–0.01 V (vs. Li^+/Li) at various current densities under the galvanostatic mode. Specific capacities were calculated based on the disk anode mass or its projected area. Cyclic voltammetry (CV) was performed with a CHI660 electrochemical workstation (CH Instruments, Shanghai) at a scanning rate of 0.1 mV s^{-1} between 3.00 and 0.01 V, and electrochemical impedance spectra (EIS) was carried out between the frequency range of 10^5 Hz and 10^{-2} Hz with an amplitude of 5 mV. Capacities were based on the total Si/C composite weight. After cycling, batteries were disassembled in the glove box and electrodes were washed with DMC thrice and dried naturally before further characterization.

3. Results and discussion

The SEM image in Fig. 2a has verified that the 3DGrSiGr is immune from the sputtering or the CVD process. The inner empty spaces and the pores among interconnected hollow branches both supply sufficient buffer for stress rearranging and electrolyte diffusion. The actual thickness of 400-nm deposition, observed from the film on the Si wafer, is ~310 nm, thinner than the diffusion limit of lithium in silicon [14]. The D, G and 2D modes of graphene as well as Si could be clearly identified in the Raman spectrum shown in Fig. 2b [15,16]. The EDS mapping reveals the discontinuously distributed Si nanoparticles over the 3DGr branches. Furthermore, the HRTEM has confirmed that the Si layer is comprised of discontinuously distributed, diamond structured Si nanoparticles with the size of about 5 nm, which can be attributed to the starting material i.e. porous 3D structure of 3DGr with unsmooth surface. The unsmooth 3DGr resulted in such a non-uniform layer of small Si nanoparticles, matching the pulverization preventing strategy of nano sized Si nanoparticles for weakening the expansion during lithiation. The structure of graphene and Si is macroscopically confirmed

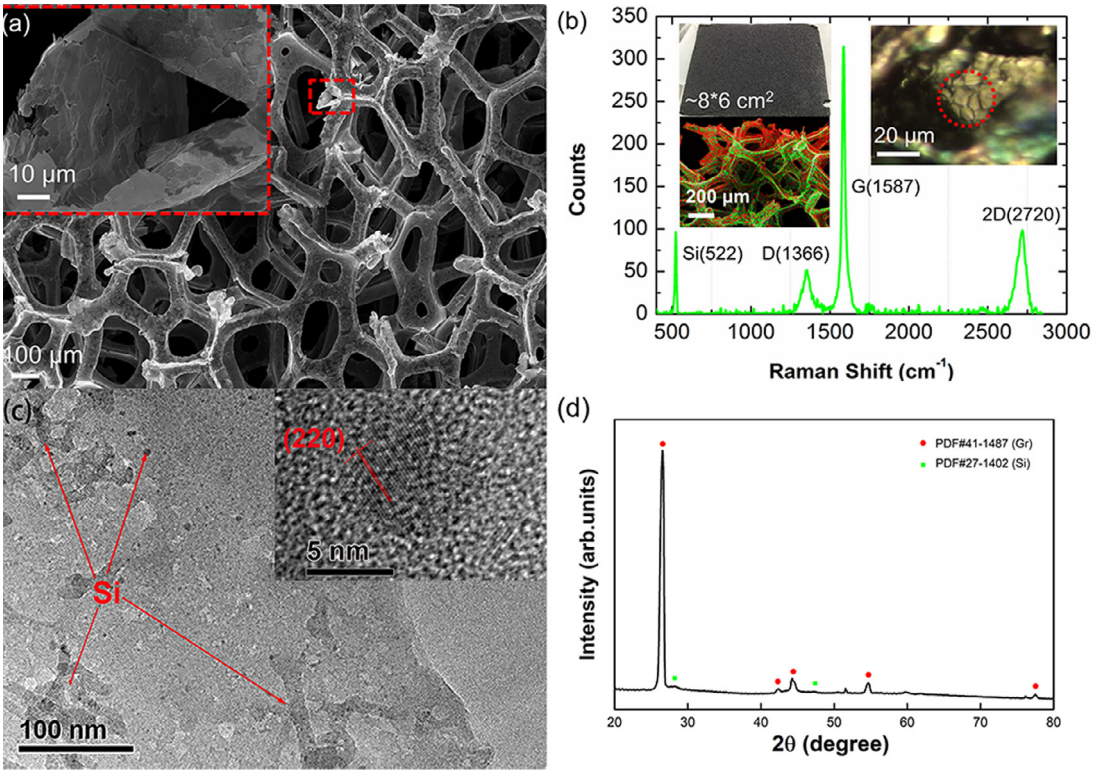

Fig. 2. (a) SEM image; (b) Raman spectrum; (c) TEM image and (d) XRD of 3DGrSiGr. The inset of (b) shows the distribution of C (red) and Si (green) via EDS mapping and optical image. The inset of (c) shows the HRTEM of Si nanoparticle with distinct (220) facets of Si diamond structure. (For interpretation of the references to color in this figure legend, the reader is referred to the web version of this article.)

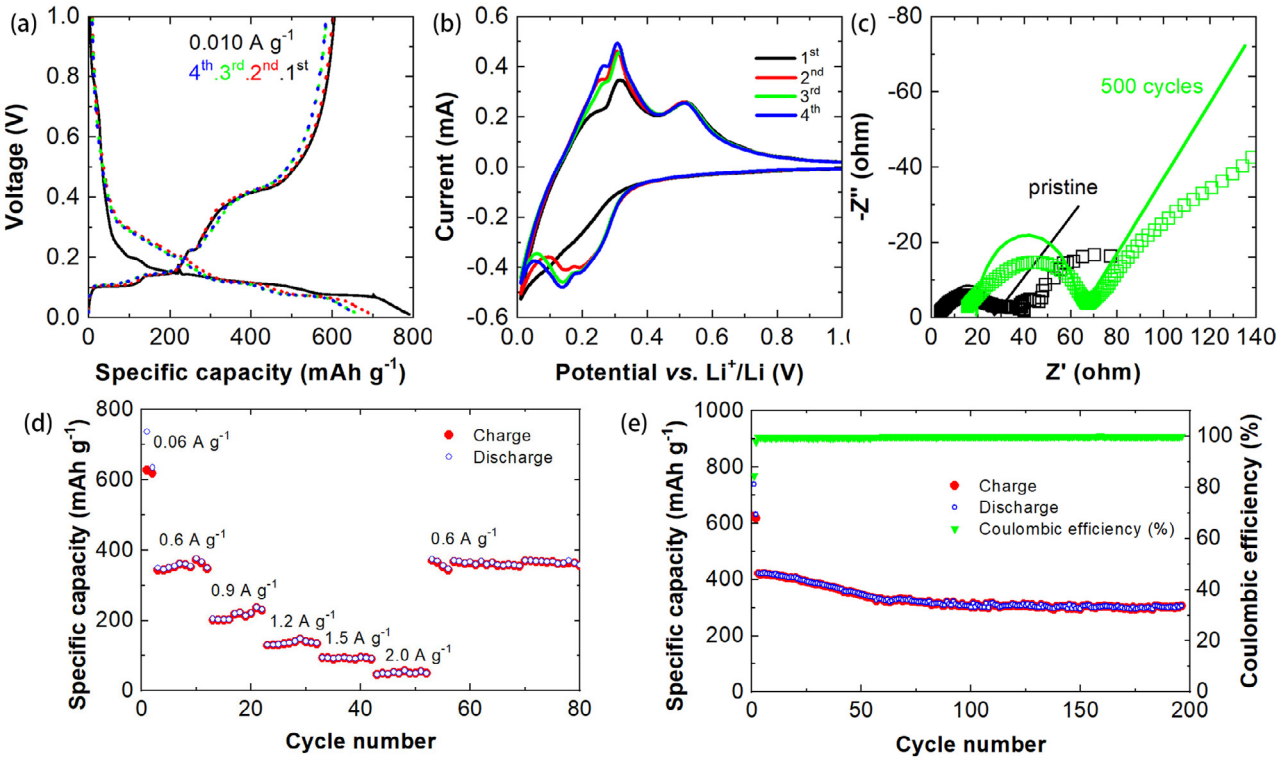

Fig. 3. (a) Voltage-capacity profiles of 3DGrSiGr anode cycled at 0.01 A g^{-1}; (b) CV curves scanned at 0.1 mV s^{-1}; (c) EIS of 3DGrSiGr before activation (black) and after 500 cycles (green) at 0.5 A g^{-1}. The marks are experimental data and the lines are fitted data; (d) Rate performance at different current densities; (e) Long-term cycling at 0.5 A g^{-1}. (For interpretation of the references to color in this figure legend, the reader is referred to the web version of this article.)

Table 1
Comparison of electrochemical performance with recent free-standing electrode works.

Structure, method	Mass load [mg cm^{-2}]	Current [mA g^{-1}]	Initial capacity [mAh g^{-1}]	Coulombic efficiency [%]	*50*th capacity [mAh g^{-1}]	Retention rate [%]	Ref.
Si film, sputtering	0.057	4620	3262	70.8	~2900	~90	25
Si film, electrodeposition	/	360	4831	~50	2800	57	26
Si-Al (~90:10) film, co-sputtering	0.35 ± 0.05	*0.05* [a]	3348	93.6	1268	38	27
Patterned Si disks, etching	~0.022	3750	3383	83.2	2205	65	28
Si/Gr NP on Gr foam, drop-casted	1.5	400	983	~60	440	45	29
Alternative Si/C/Si, sputtering	0.032	3600	~2900	61 ± 1	~2840	96 ± 2	19
Si NP + GO, co-filtration	~4	100	1650	56	1500	91	30
Si NS + rGO, LBL filtration	30%	200	2030	53	~800	~40	31
Si NP, freeze-drying	41% aerogel	50	600	60	692	115	32
	39% film	50	1040	83	~880	85	
Gr drape Si film, sputtering	0.07	1800	~3200	~85	~1750	~54	33
	0.35	3000	~2000	/	~1250	~62	
Si porous film, sputtering	0.018	1000	4104	80.5	~2900	~70	34
		20,000	~3600	~80	~2500	~70	
Si NW, suspension co-filtration	0.8~6	1000	2500 [*5~11* [b]]	~90	1700 [*6~7* [b]]	~70	35
Si film, pulsed laser deposition	0.82	*1.08* [a]	*0.12* [b]	/	*0.16* [b]	133	36
This work	0.38 (Si, 12%)	500	420	99	345	82	N/A

[a] Unit: mA cm^{-2}.
[b] Unit: mAh cm^{-2}.

Table 2
Chemical components of pristine and lithiated 3DGrSiGr (B. E.: binding energy; C. C.: chemical components).

	C 1s B. E. (eV)	C. C. [Ref.]	Si 2p B. E. (eV)	C. C. [Ref.]	O 1s B. E. (eV)	C. C. [Ref.]	Li 1s B. E. (eV)	C. C. [Ref.]
3DGrSiGr	284.5	C-sp^2 95.6% [13]	101.8	Si-C 100% [42]	532.9	Si-O 34.3% [41]	N/A	N/A
	288.5	C = O 4.4% [13]			531.5	C = O [13] O-SiC [41] 65.5%		
Lithiated 3DGrSiGr	284.1	C-sp^2 31.3% [13]	102.9	Li_xSiO_y 19.7% [40]	530.9	Si-O 84.5% [41]	53.4	Li-OH 22.9% [13]
	289.1	Li/C/O 43.1% [13]	99.5	Si-Si 43.3% [40]	532.5	Li_xSiO_y15.5% [41]	54.6	Li_xSiO_y 77.1% [41]
	285.9	Electrolyte 14.9% [41]	100.5	Li-Si 25.7% [40]				
	282.4	Si-C 10.7% [42]	101.7	Si-C 7.7% [42]				
			104.0	3.5% (weak)				

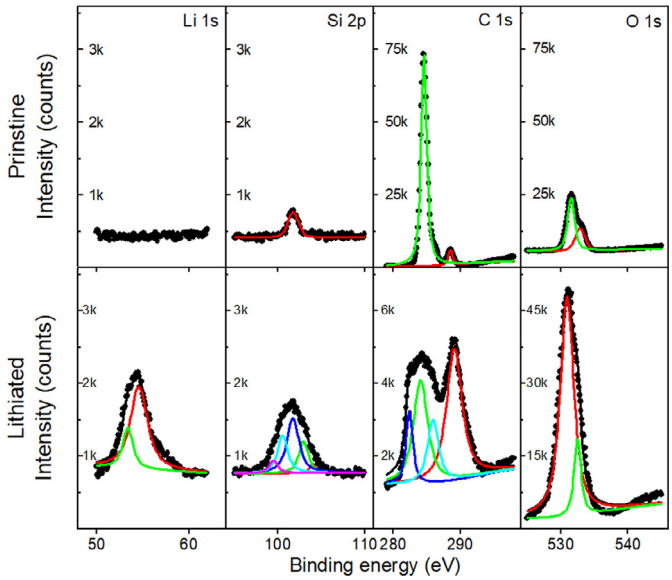

Fig. 4. XPS of the prinstine and lithiated 3DGrSiGr at Li 1 s, Si 2p, C 1 s, O 1 s, respectively.

via XRD referring to standard powder diffraction file (PDF) as shown in Fig. 2d, as well as a little residual Ni, which would not be counted into the active material.

The charge-discharge curves and CV profiles (Fig. 3) confirm both graphene and silicon contribute as active materials. A steep decreasing with a turn point near 0.70 V due to the formation of the solid electrolyte interface (SEI) layer, and a short stable period around 0.20 V from Li-Si alloying are observed in the discharging curve of the 1st cycle. Below 0.15 V the potential decreases slowly with two quasi-plateaux near 0.12 and 0.08 V observed, due to Li intercalation into graphene and the recrystallization of Li-Si alloys, respectively [17,18]. Correspondingly, Two flat regions due to the extraction of Li^+ from graphitic carbon located at 0.11 and 0.14 V are observed in the 1st charging curve, while the 0.23 V plateau and the inconspicuous flat region at 0.41 V are attributed to different stages of Li-Si dealloying [13,19]. The subsequent cycles maintain similar electrical properties except the SEI-formation turn point disappears [20], indicating good reversibility. Accordingly, during the 1st CV cycle no detecable peak is observed in the cathodic scan due to the SEI formation. Along the anodic scan broad peaks between 0.2–0.6 V arose from Li extractions from Si and C. Starting from the 2nd cycle, a peak around 0.17 V with a shoulder (~0.20 V) and another sharp peak near 0.02 V along the cathodic scan are recorded, corresponding to Li-C intercalation and Li-Si alloying [21]. Subsequently for the anodic scan, a broad peak at 0.29 V with a shoulder of 0.22 V corresponding to the amorphization of Li-Si alloys and Li extraction from graphene, respectively, as well as a weaker peak around 0.50 V due to Li extraction from various Li-Si compositions, can be identified [22]. The subsequent cycles display almost identical patterns overlapping with each other, suggesting the structural stability of the 3DGrSiGr electrodes undergoing reversible electrochemical reactions.

The Nyquist plots of a fresh cell and a 500-cycled cell shown in Fig. 3c were employed to study the electrochemical impedance. Before cycling the short-range interface resistance and intrinsic electronic resistance are 4.0 and 33.6 Ω, respectively [23]. It should be noticed that for such a freestanding sandwich structure, the starting intrinsic resistance might be influenced by the charge-transfer between graphene and Si layers. After 500 cycles at a charging density of 1.0 mA cm^{-2}, the short-range interface resistance and charge-transfer impedance increase to 15.7 and 67.6 Ω, suggesting that structures have not changed dramatically. The considerably small values are results of much enhanced ionic diffusion with the pores in the network filled with electrolyte and Li ions [13]. Galvanostatic performance of the 3DGrSiGr (3.19 mg cm^{-1} in total, where 2.81 mg cm^{-2} for graphene and 0.38 mg cm^{-2} for Si) composite is characterized at various rates after activated at 0.06 A g^{-1} for two cycles is shown in Fig. 3d. It can be observed that the specific capacities are better than the theoretical capacity of graphite [24], suggesting the Si induced improvement of power density. At the beginning of the rate performance, the 3DGrSiGr exhibits a capacity of ~360 mAh g^{-1} (1.15 mAh cm^{-2}) at 0.6 A g^{-1} (1.91 mA cm^{-2}). Although the capacity drops gradually to 50 mAh g^{-1} (0.16 mAh cm^{-2}) at 2.0 A g^{-1} (6.38 mA cm^{-2}), the coulombic efficiency maintained above 99% and the capacity returns to ~360 mAh g^{-1} after the rate performance. That stability of 3DGrSiGr suggests that Si related pulverization has been efficiently weakened. For a long-term cycling at

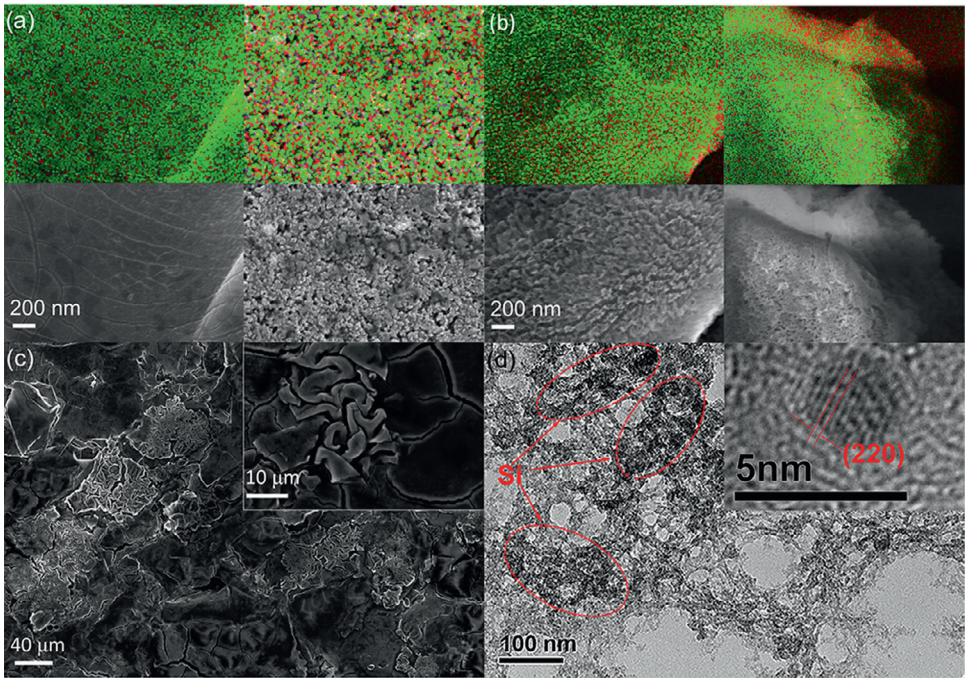

Fig. 5. SEM images and EDS mapping (Si (green) and C (red)) of 3DGrSiGr electrodes with the insets of wrinkled and cracked regions after (a) 1 cycles and (b,c) 500 cycles, respectively. (d) TEM image of cycled 3DGrSiGr with the inset of HRTEM of Si nanoparticle. (For interpretation of the references to color in this figure legend, the reader is referred to the web version of this article.)

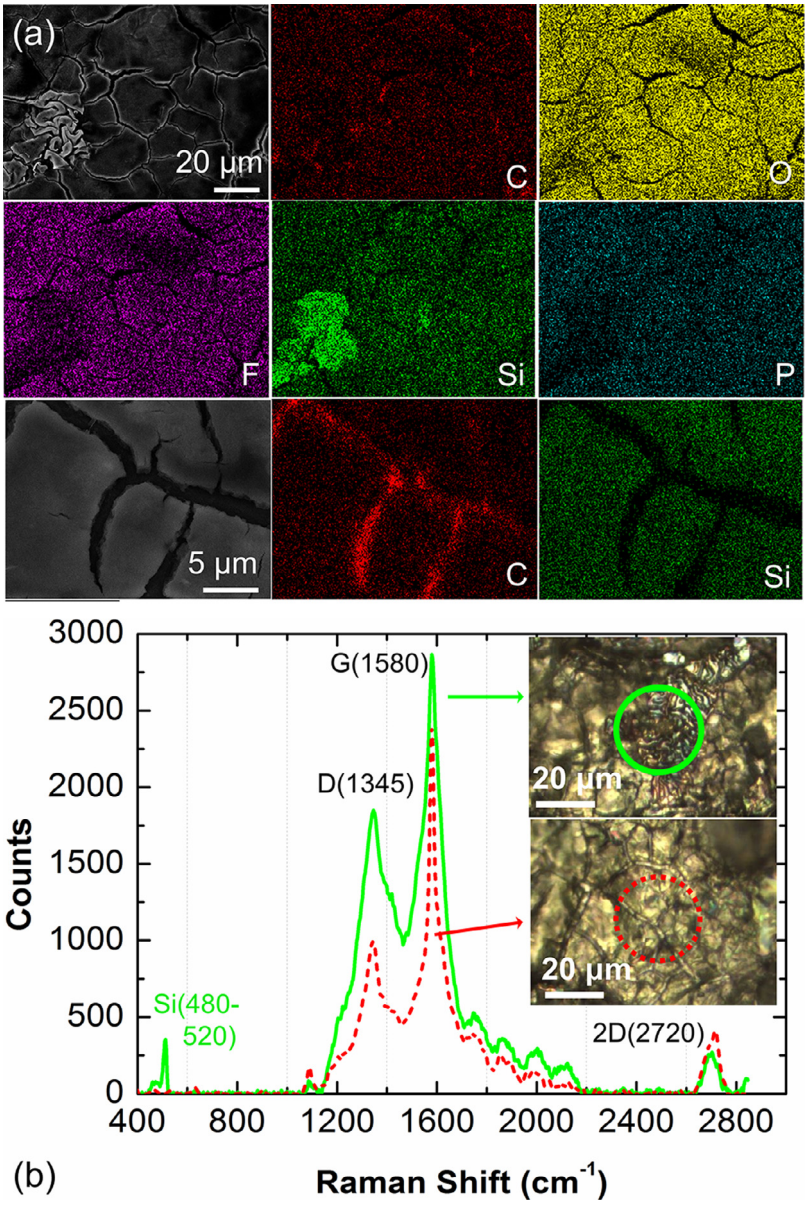

Fig. 6. (a) SEM images and EDS mapping of 3DGrSiGr after 500 cycles. The top two rows of (a) show the distribution of O, P, F, C from SEI chemicals (e.g. LiF, LixPOyFz, or ROCOOLi) and the concentrated distribution of Si over the wrinkled region. The bottom row of (a) shows the morphology and elemental distribution over the cracked region; (b) Raman spectra of 3DGrSiGr after 500 cycles. The green solid circle refers to the wrinkled region and the red dotted circle refers to the cracked region. (For interpretation of the references to color in this figure legend, the reader is referred to the web version of this article.)

0.5 A g^{-1} (1.60 mA cm^{-2}) as shown in Fig. 3e, the 3DGrSiGr exhibits a starting capacity of 420 mAh g^{-1} (1.34 mAh cm^{-2}) and maintains at 300 mAh g^{-1} (0.96 mAh cm^{-2}) after 194 cycles, showing a retention of 71%. Overall the 3DGrSiGr are able to retain a comparable capacity and very good stability referring to those low-mass active material loaded anodes (Table 1) [14,19,25–38].

The as-prepared porous 3DGrSiGr is supposed to facilitate the mass transport and provide more active sites for electrochemical reactions and thus improve the battery performance [39]. Particularly for Si in 3DGrSiGr, two important issues to be solved: how to secure the high capacity contribution of Si and how to keep the stability i.e. prevent pulverization of Si-based electrodes. Chemical features during the electrochemical lithiation of 3DGrSiGr are examined with XPS as summarized in Table 2 and Fig. 4. For a pristine 3DGrSiGr, C-sp^2, Si-C and weak oxidization of C and Si can be identified [13,40]. After lithiation, lithiated C and lithiated Si can be both extracted from XPS [41,42], indicating the cooperative contribution of C and Si to the capacity of 3DGrSiGr.

More importantly, the stability of 3DGrSiGr is critically essential to the electrochemical performance. The structural evolution during cycles is detailed investigated as shown in Fig. 5. At the beginning, the 1-cycled 3DGrSiGr exhibits similar surface morphology and uniform Si distribution to a fresh 3DGrSiGr, as shown in Fig. 5a. After 500 cycles, the 3DGrSiGr has maintained the flexibility as a whole piece by appearance, while at microscale a few morphological defects such as wrinkles and cracks pulverizing the anode are observed, as shown in Fig. 5(b, c). So it can be concluded that 3DGrSiGr has experienced a slow structural evolution during the cycling, which guarantees the electrochemical stability. The EDS mapping also reveals a discrete and uniform distribution for cycled 3DGrSiGr, corresponding to a stable and reversible performance of lithiation and delithiation. Although Si nanoparticles in the cycling 3DGrSiGr have the trend to accumulate as shown in EDS mapping and TEM image, this process would be quite slow and small Si nanoparticles can still be identified as the HRTEM

image in the inset of Fig. 5d describes. The EDS mapping in a large area and Raman spectra of cycled 3DGrSiGr (Fig. 6) has further exhibited an intensive Si signal in the wrinkled region, in reflection of the gathering of Si nanoparticles in the wrinkled region during lithiation and delithiation, which might indicate that the native morphological defects in a 3DGr provide additional buffering spaces [13] to compensate the volume expansion induced by the lithiation of Si. Moreover, the coverage of outer layer of graphene on the Si nanoparticles layer can prevent the desorption of Si nanoparticles i.e. the loss of active materials and further increase the electrical continuity, stabilizing the battery performances. The functions of 3DGr and Si nanoparticles in 3DGrSiGr can be summarized as follows: the 3DGr provides a porous, flexible and 3D architecture for Si nanoparticles, serving as the buffering and stabilizing support, the current collector, and a part of active materials; the Si nanoparticles further increases the capacity. The small sizes of Si nanoparticles, the flexibility, porous 3D structure and morphological defects of 3DGr act synergistically to avoid pulverization for such a Si-based anode.

4. Conclusions

In summary, a Si/C hybrid network building up a microscale sandwich structure on the surface of 3DGr is proposed. The 3DGr forms an interconnected skeleton, acting as an active material, as well as a buffering support and current collector for Si, while Si nanoparticles further contribute to the electrochemical performance. Synergistically, the small sizes of Si nanoparticles, the flexibility, porous 3D structure and morphological defects of 3DGr work together to avoid pulverization for such a Si-based anode and thus facilitate the cycling stability.

Declaration of Competing Interests

The authors declare that they have no known competing financial interests Or personal relationships that could have appeared to influence the work reported in this paper.

Acknowledgments

The authors thank NSF of Fujian Province, China (No. 2017J01103) and the Graphene Project of Fujian Provincial Development and Reform Commission. The project is also funded by NSFC (Nos. 21303143, 11574255), and the Department of Education of Fujian Province (No. JAT170012). Ms. Lingling Zheng is sincerely appreciated for her support with material characterizations.

References

[1] J.W. Choi, D. Aurbach, Promise and reality of post-lithium-ion batteries with high energy densities, Nat. Rev. Mater. 1 (2016) 16013.
[2] U. Kasavajjula, C. Wang, A.J. Appleby, Nano- and bulk-silicon-based insertion anodes for lithium-ion secondary cells, J. Power Sources 163 (2007) 1003–1039.
[3] Y. Liu, G. Zhou, K. Liu, Y. Cui, Design of complex nanomaterials for energy storage: past success and future opportunity, Acc. Chem. Res. 50 (2017) 2895–2905.
[4] R. Dash, S. Pannala, Theoretical limits of energy density in silicon-carbon composite anode based lithium ion batteries, Sci. Rep. 6 (2016) 27449.
[5] X.H. Shen, Z.Y. Tian, R.J. Fan, L. Shao, D.P. Zhang, G.L. Cao, L. Kou, Y.Z. Bai, Research progress on silicon/carbon composite anode materials for lithium-ion battery, J. Energy Chem. 27 (2018) 1067–1090.
[6] Q. Xu, J.Y. Li, J.K. Sun, Y.X. Yin, L.J. Wan, Y.G. Guo, Watermelon-inspired Si/C microspheres with hierarchical buffer structures for densely compacted lithium-ion battery anodes, Adv. Energy. Mater 7 (2017) 1601481.
[7] Y.Z. Li, K. Yan, H.W. Lee, Z.D. Lu, N. Liu, Y. Cui, Growth of conformal graphene cages on micrometre-sized silicon particles as stable battery anodes, Nat. Energy 1 (2016) 15029.
[8] X.W. Zhong, Z.Z. Yang, X.W. Liu, J.Q. Wang, L. Gu, Y. Yu, General strategy for fabricating sandwich-like graphene-based hybrid films for highly reversible lithium storage, ACS Appl. Mater. Interfaces 7 (2015) 18320–18326.
[9] S. Choi, T.W. Kwon, A. Coskun, J.W. Choi, Highly elastic binders integrating polyrotaxanes for silicon microparticle anodes in lithium ion batteries, Science 357 (2017) 279–283.
[10] Z.P. Chen, W.C. Ren, L.B. Gao, B.L. Liu, S.F. Pei, H.M. Cheng, Three-dimensional flexible and conductive interconnected graphene networks grown by chemical vapour deposition, Nat. Mater. 10 (2011) 424–428.
[11] S. Suresh, Z.P. Wu, S.F. Bartolucci, S. Basu, R. Mukherjee, T. Gupta, P. Hundekar, Y. Shi, T.M. Lu, N. Koratkar, Protecting silicon film anodes in lithium-ion batteries using an atomically thin graphene drape, ACS Nano. 11 (2017) 5051–5061.
[12] S. Basu, S. Suresh, K. Ghatak, S.F. Bartolucci, T. Gupta, P. Hundekar, R. Kumar, T.M. Lu, D. Datta, Y. Shi, N. Koratkar, Utilizing van der waals slippery interfaces to enhance the electrochemical stability of silicon film anodes in lithium-ion batteries, ACS Appl. Mater. Interfaces 10 (2018) 13442–13451.
[13] H.C. Guo, D. Long, Z.Z. Zheng, X.Y. Chen, A.M.C. Ng, M. Lu, Defect-enhanced performance of a 3D graphene anode in a lithium-ion battery, Nanotechnology 28 (2017) 505402.
[14] F. Farmakis, C. Elmasides, P. Fanz, M. Hagen, N. Georgoulas, High energy density amorphous silicon anodes for lithium ion batteries deposited by DC sputtering, J. Power Sources 293 (2015) 301–305.
[15] Z. Iqbal, S. Veprek, Raman scattering from hydrogenated microcrystalline and amorphous silicon, J. Phys. C 15 (1982) 377–392.
[16] A.C. Ferrari, J.C. Meyer, V. Scardaci, C. Casiraghi, M. Lazzeri, F. Mauri, S. Piscanec, D. Jiang, K.S. Novoselov, S. Roth, A.K. Geim, Raman spectrum of graphene and graphene layers, Phys. Rev. Lett. 97 (2006) 187401.
[17] M.K. Datta, P.N. Kumta, In situ electrochemical synthesis of lithiated silicon–carbon based composites anode materials for lithium ion batteries, J. Power Sources 194 (2009) 1043–1052.
[18] L.W. Ji, H.H. Zheng, A. Ismach, Z.K. Tan, S.D. Xun, E. Lin, V. Battaglia, V. Srinivasan, Y.G. Zhang, Graphene/Si multilayer structure anodes for advanced half and full lithium-ion cells, Nano Energy 1 (2012) 164–171.
[19] A.R. Jiménez, R. Klöpsch, R. Wagner, U.C. Rodehorst, M. Kolek, R. Nölle, M. Winter, T. Placke, A step toward high-energy silicon-based thin film lithium ion batteries, ACS Nano 11 (2017) 4731–4744.
[20] L. Gan, H.J. Guo, Z.X. Wang, X.H. Li, W.J. Peng, J.X. Wang, A facile synthesis of graphite/silicon/graphene spherical composite anode for lithium-ion batteries, Electrochim. Acta 104 (2013) 117–123.
[21] M. Choi, J.C. Kim, D.W. Kim, Waste windshield-derived silicon/carbon nanocomposites as high-performance lithium-ion battery anodes, Sci. Rep. 8 (2018) 960.
[22] Y. Yao, M.T. McDowell, I. Ryu, H. Wu, N. Liu, L. Hu, W.D. Nix, Y. Cui, Interconnected silicon hollow nanospheres for lithium-ion battery anodes with long cycle life, Nano Lett. 11 (2011) 2949–2954.
[23] J.Y. Song, H.H. Lee, Y.Y. Wang, C.C. Wan, Two- and three-electrode impedance spectroscopy of lithium-ion batteries, J. Power Sources 111 (2002) 255–267.
[24] E. Yoo, J. Kim, E. Hosono, H.S. Zhou, T. Kudo, I. Honma, Large reversible Li storage of graphene nanosheet families for use in rechargeable lithium ion batteries, Nano Lett. 8 (2008) 2277–2282.
[25] G. Schmuelling, M. Winter, T. Placke, Investigating the Mg–Si binary system via combinatorial sputter deposition as high energy density anodes for lithium-ion batteries, ACS Appl. Mater. Interfaces 7 (2015) 20124–20133.
[26] G.Y. Zhao, Y.F. Meng, N.Q. Zhang, K.N. Sun, Electrodeposited Si film with excellent stability and high rate performance for lithium-ion battery anodes, Mater. Lett. 76 (2012) 55–58.
[27] P. Liu, J.J. Zheng, Y.M. Qiao, H. Li, J.M. Wang, M.C. Wu, Fabrication and characterization of porous Si-Al films anode with different macroporous substrates for lithium-ion batteries, J. Solid State Electrochem. 18 (2014) 1799–1806.
[28] Y. He, X.Q. Yu, Y.H. Wang, H. Li, X.J. Huang, Alumina-coated patterned amorphous silicon as the anode for a lithium-ion battery with high coulombic efficiency, Adv. Mater. 23 (2011) 4938–4941.
[29] J.J. Ji, H.X. Ji, L.L. Zhang, X. Zhao, X. Bai, X.B. Fan, F.B. Zhang, R.S. Ruoff, Graphene-encapsulated Si on ultrathin-graphite foam as anode for high capacity lithium-ion batteries, Adv. Mater. 25 (2013) 4673–4677.
[30] H. Jiang, X. Zhou, G.G. Liu, Y.H. Zhou, H.Q. Ye, Y. Liu, K. Han, Free-standing Si/graphene paper using Si nanoparticles synthesized by acid-etching Al-Si alloy powder for high-stability Li-ion battery anodes, Elctrochim. Acta 188 (2016) 777–784.
[31] H.X. Zhang, S.L. Jing, Y.J. Hu, H. Jiang, C.Z. Li, A flexible freestanding Si/rGO hybrid film anode for stable Li-ion batteries, J. Power Sources 307 (2016) 214–219.
[32] C. Botas, D. Carriazo, W. Zhang, T. Rojo, G. Singh, Silicon-reduced graphene oxide self-standing composites suitable as binder-free anodes for lithium-ion batteries, ACS Appl. Mater. Interfaces 8 (2016) 28800–28808.
[33] S. Suresh, Z.P. Wu, S.F. Bartolucci, S. Basu, R. Mukherjee, T. Gupta, P. Hundekar, Y. Shi, T.M. Lu, N. Koratkar, Protecting silicon film anodes in lithium-ion batteries using an atomically thin graphene drape, ACS Nano 11 (2017) 5051–5061.
[34] L. Lin, Y.T. Ma, Q.S. Xie, L.S. Wang, Q.F. Zhang, D.L. Peng, Copper-nanoparticle-induced porous Si/Cu composite films as an anode for lithium ion batteries, ACS Nano 11 (2017) 6893–6903.
[35] R.V. Salvatierra, A.R.O. Raji, S.K. Lee, Y. Ji, L. Li, J.M. Tour, Silicon nanowires and lithium cobalt oxide nanowires in graphene nanoribbon papers for full lithium ion battery, Adv. Energy Mater. 6 (2016) 1600918.
[36] E. Biserni, A. Scarpellini, A. Li Bassi, P. Bruno, Y. Zhou, M. Xie, High-performance flexible nanoporous Si-carbon nanotube paper anodes for micro-battery applications, Nanotechnology 27 (2016) 245401.
[37] M. Ashuri, Q.R. He, L.L. Shaw, Silicon as a potential anode material for Li-ion batteries: where size, geometry and structure matter, Nanoscale 8 (2016) 74–103.
[38] A. Mukanova, A. Nurpeissova, A. Urazbayev, S.S. Kim, M. Myronov, Z. Bakenov, Silicon thin film on graphene coated nickel foam as an anode for Li-ion batteries, Electrochim. Acta 258 (2017) 800.
[39] K. Feng, W. Ahn, G. Lui, H.W. Park, A.G. Kashkooli, G.P. Jiang, X.L. Wang, X.C. Xiao, Z.W. Chen, Implementing an in-situ carbon network in Si/reduced graphene oxide for high performance lithium-ion battery anodes, Nano Energy 19

(2016) 187–197.
[40] E. Radvanyi, E. De Vito, W. Porcher, S. Jouanneau Si Larbi, An XPS/AES comparative study of the surface behaviour of nano-silicon anodes for Li-ion batteries, J. Anal. At. Spectrom. 29 (2014) 1120–1131.
[41] C. Pereira-Nabais, J. Swiatowska, A. Chagnes, F. Ozanam, A. Gohier, P. Tran-Van, C. Cojocaru, M. Cassir, P. Marcus, Interphase chemistry of Si electrodes used as anodes in Li-ion batteries, Appl. Surf. Sci 266 (2013) 5–16.
[42] S. Tengeler, B. Kaiser, G. Ferro, D. Chaussende, W. Jaegermann, The (001) 3C SiC surface termination and band structure after common wet chemical etching procedures, stated by XPS, LEED, and HREELS, Appl. Surf. Sci 427 (2018) 480–485.